IET Generation, Transmission & Distribution

Research Article

IET Journals
The Institution of Engineering and Technology

Series impedance of distribution cables with sector-shaped conductors

ISSN 1751-8687
Received on 26th April 2015
Revised on 3rd June 2015
Accepted on 18th June 2015
doi: 10.1049/iet-gtd.2015.0546
www.ietdl.org

Andrew J. Urquhart ✉, *Murray Thomson*

Centre for Renewable Energy Systems Technology (CREST), School of Electronic, Electrical and Systems Engineering, Loughborough University, Loughborough LE11 3TU, UK
✉ *E-mail: a.j.urquhart@lboro.ac.uk*

Abstract: Models of power distribution networks require accurate cable impedance data. For unbalanced networks, both the self-impedances and the mutual impedances are needed. However, published studies use differing approaches to determine cable impedances, leaving uncertainty over the level of detail required. This study compares impedances provided by the manufacturer with those from several analytical methods, showing the impact of modelling the non-circular geometry and of including corrections allowing for the AC resistance. The analysis is compared to results from a freely available finite element (FE) solver where the current distribution is modelled in detail, taking account of eddy currents and the rotation of the cores relative to the neutral due to the cable lay. At 50 Hz, the analytical methods provide a good approximation, but the FE results show that eddy currents affect the impedance at harmonic frequencies. The results also show the impact of including the ground path in the impedance calculation. The current distribution in the ground has a wide cross-sectional area, suggesting that the assumption of a perfect multi-grounded neutral is inappropriate for low voltage networks with short cable lengths.

1 Introduction

Low-carbon technologies such as electric vehicles, heat pumps and solar photovoltaic panels are increasingly being connected to the low voltage (LV) distribution network. This may lead to voltages at customer connections being outside of their permitted ranges. Accurate modelling is therefore needed to ensure that cables are correctly sized and to determine whether connections of new technologies can be permitted. This requires accurate series impedance data for the cables.

The uneven allocation of customers to the three phases and the stochastic nature of their demands causes the currents to be highly unbalanced [1]. This unbalance is likely to be worsened by the addition of large single-phase low-carbon technologies. Models of these unbalanced networks require data for both the self-impedance and mutual impedance of the cables. Since the neutral conductor may be grounded at multiple locations along the feeder, the ground path is frequently also included [2].

Increasing levels of harmonics also cause concern due to the need to meet voltage distortion metrics and due to the increased losses and heating effects, particularly in the neutral conductor [3]. Impedance data is therefore also required for harmonic frequencies.

Data from cable manufacturers is not always sufficient to derive the full frequency-dependent matrix with self- and mutual impedance terms [4]. The impact of the ground path is normally excluded as this varies with local ground resistivity and depends on the location of earth electrodes. In response to this lack of data, a number of techniques have previously been used to estimate the impedances.

In some studies, the impedance is specified as a single complex value without defining the mutual impedances [5, 6]. In other cases, the impedance is defined to be the positive sequence term and the zero sequence term is then approximated by applying a scaling factor of between 3 and 5 to the positive sequence [7, 8]. However, voltage calculations for unbalanced demands are sensitive to this uncertain scaling factor [8]. This approximation also provides a symmetrical phase impedance matrix and is equivalent to assuming that the phases are fully transposed, potentially introducing further errors in voltage and loss calculations [9].

Other studies have utilised software tools such as OpenDSS [10] or DIgSILENT [11]. These tools allow for cable impedances to be determined using Carson's equations [12] where a ground path can be included, typically assuming a perfect multi-grounded neutral with zero voltage between the neutral and the ground. Carson's equations were intended for widely spaced overhead lines, but are also employed for underground cables (with some uncertainty, as in [2]). A modified form of Carson's equations is commonly used to reduce the computational complexity [13] and the errors introduced by the approximation have been found to be negligible for underground cables [14].

These approaches typically assume a uniform current distribution within the cable conductors, neglecting induced eddy currents and so not allowing for the skin effect or the proximity effect with closely spaced conductors. Analytical expressions for the skin effect are available for circular conductors [15] and an analysis has also been developed for the proximity effect in a cable with four sectors [16]. Studies of harmonics have used correction factors for the AC resistance from IEC 60287 [17, 18] although these do not allow for the many variations in the structures of the sector-shaped conductors and cable lay.

Finite element (FE) methods have been developed to provide a more accurate model of the current distribution within the conductors, and modern computing allows these models to include the ground surrounding the cable [19]. A hybrid approach was taken in [20] where the current distribution within the cable was solved using a numerical method, combined with corrections from [15] for the ground path. These techniques may provide a high degree of accuracy, but tend to be complex to apply and published models for specific cable types cannot easily be adapted for new applications.

The use of this wide range of different approaches suggests that there is some uncertainty over the level of detail needed so that impedances are adequately represented. This paper, therefore reviews the underlying theory (Section 2), and evaluates the differences between modelling approaches for the example case of

waveform cable (Section 3). Four analytical calculation methods are compared, progressively adding more detail to the model (Section 4). The use of a freely available FE solver is introduced (Section 5) and results are compared with those from the analysis (Section 6). The impedance data is available for download [21].

This paper does not include calculation of shunt admittance due to capacitance, because its effect is small relative to that of series impedance, in the context of LV distribution networks at 50 Hz. The phase-to-neutral admittance is calculated in [13] for a single core cable with similar concentric neutral dimensions to the waveform cable considered here as 60 μS/km, giving currents at 230 V of just 14 mA/km. The phase-to-phase capacitance in sector cables has also been measured at around 75 nF/km, or 24 μS/km at 50 Hz [22]. At higher voltages and harmonic frequencies, however, capacitance does become significant. It may be estimated assuming circular conductors and uniform charge density or, for greater accuracy, FE models using similar concepts to those presented in this paper could be developed.

2 Impedance definitions

2.1 Conductor impedances

The cable can be modelled as a set of conductors with associated self- and mutual impedances, as shown in Fig. 1. This shows two conductors i and j and a ground conductor g. The equivalent circuit is shorted together at one end to represent only the voltage drops due to the cable (excluding those due to the loads).

By assuming a uniform current distribution (neglecting eddy currents), the conductor resistances can be calculated based on their cross-sectional area and resistivity. The inductances include contributions due to the flux linkage that is internal to the conductor, and also due to the external flux linkage. The external flux linkage can be obtained by integrating the magnetic field from the conductor surface at radius R to a point P. In the case of the FE model described below in Section 5, this represents the distance to the boundary of the finite solution area.

Following the established approach as outlined by Glover *et al.* [23], if the magnetic field is considered to a finite distance P, the total flux linkage for conductor i with a total of N_{cond} conductors is

$$\lambda_{iP} = \frac{\mu_0}{2\pi} \sum_{j=1}^{N_{\text{cond}}} I_j \ln \frac{D_{Pj}}{D_{ij}} \tag{1}$$

where D_{Pj} is the distance from conductor j to point P and D_{ij} is the geometric mean distance (GMD) between conductors i and j. For $i = j$, the distance D_{ii} is the geometric mean radius (GMR) of conductor i. The GMR of a circular conductor is given by $D_{ii} = \mathrm{e}^{-1/4}R$ where R is the physical radius.

The GMD can be determined by considering each conductor to be formed from a set of sub-conductors, each having uniform current density and carrying an equal share of the total current. The GMD can then be calculated as

$$D_{ij} = \mathrm{e}^{\left(\sum_{m=1}^{N_{\text{sub},j}} \sum_{k=1}^{N_{\text{sub},i}} \ln d_{mk}\right) / \left(N_{\text{sub},j} N_{\text{sub},i}\right)} \tag{2}$$

where $N_{\text{sub},i}$ is the number of sub-conductors in conductor i. When $k = m$, distance d_{km} is the GMR of one sub-conductor. Otherwise when $k \neq m$, distance d_{mk} is strictly defined as the GMD between the sub-conductors [24]. However, this gives a recursive definition and the centre-to-centre distance between the sub-conductors is used instead. This gives a negligible error provided that the sub-conductors are small compared to the distances between them. For a high density of sub-conductors, the formulation of (2) using the arithmetic mean of logarithms is less subject to numerical rounding errors than the direct calculation of the geometrical mean as in [23].

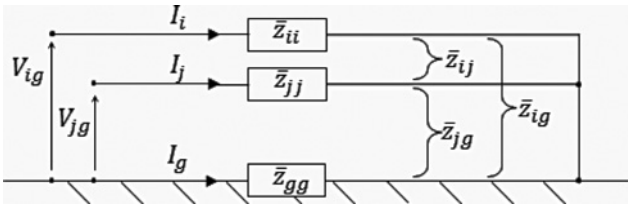

Fig. 1 *Conductor impedance model*

2.2 Circuit impedances

It is generally assumed that the conductors belong to circuits where the sum of currents in the cable and the ground is zero. As the distance to point P tends to infinity, the total magnetic field then tends to zero [23]. The terms in (1) relating to distance D_{Pj} then cancel and the total flux linkage is

$$\lambda_{iP} = \mu_0/(2\pi) \sum_{m=1}^{M} I_m \ln(1/D_{im}) \tag{3}$$

Taking the self- or mutual inductance of a conductor as the component of (3) proportional to the corresponding current, the conductor impedances can be expressed as

$$\bar{z}_{ii} = r_i + \mathrm{j}(\omega\mu_0/(2\pi)) \cdot \ln(1/D_{ii}) \tag{4}$$

$$\bar{z}_{ij} = \mathrm{j}(\omega\mu_0/(2\pi)) \cdot \ln(1/D_{ij}) \tag{5}$$

where r_i is the resistance of conductor i in Ω/m, and ω is the angular frequency. Although (4) and (5) appear to be properties of individual conductors, they are more correctly contributions from each conductor to the total impedance of a circuit.

The circuit impedance is commonly represented as a single parameter, following the method of [13]. Referring to Fig. 1, Kirchoff's voltage law for V_{ig} gives

$$V_{ig} = \bar{z}_{ii}I_i + \bar{z}_{ij}I_j + \bar{z}_{ig}I_g - \bar{z}_{gi}I_i - \bar{z}_{gj}I_j - \bar{z}_{gg}I_g \tag{6}$$

With the sum of currents equal to zero such that $I_g = -(I_i + I_j)$, this can be written

$$V_{ig} = \hat{z}_{ii}I_i + \hat{z}_{ij}I_j \tag{7}$$

in which the circuit impedances are defined as

$$\hat{z}_{ii} = \bar{z}_{ii} - \bar{z}_{gi} - \bar{z}_{ig} + \bar{z}_{gg} \tag{8}$$

$$\hat{z}_{ij} = \bar{z}_{ij} - \bar{z}_{gj} - \bar{z}_{ig} + \bar{z}_{gg} \tag{9}$$

For circuits with a ground return path where the distance to the equivalent ground conductor is unknown, the circuit impedances in Ω/m can be calculated using Carson's equations. Using the modified equations from [13] in SI units, these are

$$\hat{z}_{ii} = r_i + \mu_0\omega/8 + \mathrm{j}\mu_0\omega/(2\pi) \cdot \ln\left(658.9/\left(D_{ii}\sqrt{f/\rho}\right)\right) \tag{10}$$

$$\hat{z}_{ij} = \mu_0\omega/8 + \mathrm{j}\mu_0\omega/(2\pi) \cdot \ln\left(658.9/\left(D_{ij}\sqrt{f/\rho}\right)\right) \tag{11}$$

where ρ is the ground resistivity in Ωm.

These circuit impedances are dependent on the assumption noted above that the total current sums to zero, but this may not be strictly accurate in meshed networks where feeders are looped. A mesh configuration can arise in LV networks where the neutrals remain permanently connected at link boxes, even if the network is considered radial with regard to the phase conductors.

Table 1 Parameters for 3-core 95 mm^2 cable [25, 26], with DC resistances are quoted at 20°C

sector area, a	92.14 mm^2	insulation thickness, t	1.1 mm
sector radius, b	10.24 mm	number of strands, N_S	30
corner radius, c	1.02 mm	neutral strand radius, R_S	0.79 mm
sector width, w	15.76 mm	neutral radius, R_N	14.36 mm
sector angle, ϕ	119°	neutral resistance	0.32 Ω/km
sector depth, s	9.14 mm	outer radius, R_O	17.25 mm
sector lay length	800 mm	neutral lay length	>250 mm
sector resistance	0.32 Ω/km		

2.3 Phase and sequence impedances

Where the ground path is included in the impedance matrix, the ground currents depend on the earthing method. The neutral and ground may be isolated (for networks with independent earths), or may be connected at a number of earth electrodes (as with protective multiple earthing). Typically the impedance of these grounding connections is high compared to that of the cable [2].

A multi-grounded neutral can be modelled by assuming a short circuit between the neutral and the ground at each node [13]. The Kron reduction can then be applied to the circuit impedance matrix, to give a 3×3 phase impedance matrix $\boldsymbol{z}_{abc}$ [13]. This can be transformed to give a 3×3 sequence impedance matrix $\boldsymbol{z}_{012}$. For a cable with rotational symmetry between phases, the impedances are then fully represented by the zero and positive sequence impedances.

3 Waveform cable

Impedance calculation methods are compared here for waveform cables, designed for underground use in LV networks. The cable consists of either 3 or 4 aluminium sector conductors surrounded by copper concentric neutral/earth conductor, as described in Table 1 and Fig. 2.

The nominal cable design is standardised [25–27], but dimensions such as the insulation thickness may be greater than the specified minimum to allow for manufacturing tolerances. The standards have evolved over the years and newer editions require fewer copper strands, but with increased diameter to maintain the overall resistance. Installed cables (possibly several decades in age) may therefore differ from those in current product datasheets.

The sector conductors have a cable lay, rotating about the central axis of [27]. The lay length is long in comparison to the width and radial offset of the sector and so the total conductor length is approximately equal to that of the cable. The neutral strands have a shorter lay length with an approximately sinusoidal waveform (rather than a continuously advancing rotation). Along the length of the cable, the sector cores therefore rotate relative to the neutral strands.

Impedance data for the cable is shown in Table 2, where the manufacturer's data is interpreted as a contribution from each conductor to the circuit impedance. In this example, the impedance of the neutral conductor is assumed to equal that of the phase conductor (typically the case for the resistance, although not necessarily so for the reactance). The table shows the implied impedances from (8) and (9) for circuits with the neutral as the return path (the cable is isolated from the ground). The terms here are double the individual conductor impedances, allowing for the circuit loop through the sector core and neutral return. In the corresponding sequence impedance matrix, the positive sequence term is then equal to the individual conductor impedance. The zero sequence term is exactly four times the positive sequence.

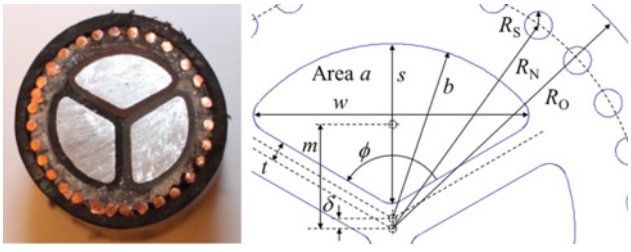

Fig. 2 *Sample cross-section of 3-core 95 mm^2 cable and dimensions*

Table 2 Impedances based on manufacturer's data for 3-core 95 mm^2 cable

Manufacturer provided data:	
DC resistance at 20°C	$r = 0.32$ Ω/km
approximate reactance at 50 Hz	$x = 0.0735$ Ω/km

Implied conductor impedance matrix, Ω/km

$$\bar{\boldsymbol{z}} = \begin{bmatrix} 0.32 + \text{j}0.0735 & 0 & 0 & 0 \\ 0 & 0.32 + \text{j}0.0735 & 0 & 0 \\ 0 & 0 & 0.32 + \text{j}0.0735 & 0 \\ 0 & 0 & 0 & 0.32 + \text{j}0.0735 \end{bmatrix}$$

Circuit impedance matrix with neutral as return path, no ground path, Ω/km

$$\hat{\boldsymbol{z}} = \begin{bmatrix} 0.64 + \text{j}0.147 & 0 + \text{j}0.0735 & 0 + \text{j}0.0735 \\ 0 + \text{j}0.0735 & 0.64 + \text{j}0.147 & 0 + \text{j}0.0735 \\ 0 + \text{j}0.0735 & 0 + \text{j}0.0735 & 0.64 + \text{j}0.147 \end{bmatrix}$$

Phase impedance matrix with no ground path $\boldsymbol{z}_{abc} = \hat{\boldsymbol{z}}$

Sequence impedance matrix with neutral as return path, no ground path, Ω/km

$$\boldsymbol{z}_{012} = \begin{bmatrix} 1.28 + \text{j}0.294 & 0 & 0 \\ 0 & 0.32 + \text{j}0.0735 & 0 \\ 0 & 0 & 0.32 + \text{j}0.0735 \end{bmatrix}$$

4 Analytical methods

4.1 Approximating sector shapes as circular

The impedances derived from the manufacturer's data are now compared with impedances from several analytical techniques. A simple estimate of the impedance can be made with the conductors approximated as being circular [28]. The cable lay is neglected in this approach.

The GMR of the sector is assumed to be that of a circle with the same area a

$$D_{ii} = \text{e}^{-1/4}\sqrt{a/\pi} \tag{12}$$

The distances between sectors are calculated relative to a nominal centre at distance m from the cable axis, as shown in Fig. 2 given by

$$m = b - s/2 + \delta \tag{13}$$

The centre of rotation of the sector arcs may be displaced slightly from the centre axis of the cable assembly (as discussed in [21]). This increases the gaps between sectors to allow for the thickness of their insulation sleeves. The offset δ is given by

$$\delta \cong t/\sin(\theta_{12}/2) - b + s + c(1/\sin(\phi/2) - 1) \tag{14}$$

where θ_{12} is the angular separation between two adjacent sectors (120° for a 3-core cable).

The GMD between sectors is approximated by the distance between their nominal centres, given by

$$D_{ij} = m\sqrt{(1 - \cos\theta_{ij})^2 + \sin^2\theta_{ij}} \tag{15}$$

The GMD between a sector and the neutral can be found from (2), where the strands comprise the sub-conductors in the neutral and with the sector represented as a single conductor at distance m from the cable centre.

The GMR of the neutral could be also found from (2), but for a ring of circular conductors is obtained more easily from

$$D_{nn} = \sqrt[N_S]{R'_S \cdot N_S \cdot R_N^{N_S-1}} \tag{16}$$

where $R'_S = e^{-1/4} R_S$ is the GMR of one strand [13].

The impedances for circuits with a neutral return path can then be determined by applying (4) and (5), giving the results as shown in Table 3.

4.2 Modelling sectors using multiple sub-conductors

The results above are now compared with those for a more detailed model of the sector geometry, in which the sector shapes are represented by a set of sub-conductors in parallel. This provides an improved estimate of the GMR and GMD parameters without needing the approximations for a nominal centre point of the sector shape. The current distribution is still assumed to be uniform, both within each sub-conductor and across the sector shape.

The method used to define the outline of the sector shape is described in detail in [21]. A rectangular grid of sub-conductors is defined within this outline, as shown in Fig. 3. Each sub-conductor is assumed to be a square with a GMR of 0.447 times the side length [24]. The neutral strands do not require further sub-division since they are circular and their GMR is already known.

The GMR and GMD parameters of the combined sector and neutral conductors can then be determined using (2). This provides a 4×4 matrix D_{ij}, equivalent to that derived in Section 4.1. Compared to the approximation using circular conductors, the sub-conductor method gives a slight increase in the GMR of a sector (from 4.2 to 4.4 mm) and also an increase in the GMD between sectors (from 10.4 to 11.6 mm).

The circuit equations are applied as above, to derive the sequence impedances included in Table 3. Compared to the simpler method of Section 4.1, there is a 14% decrease in the zero sequence reactance and a 7% increase in the positive sequence reactance. The resistances are unaffected since the conductor areas are equal in both cases and the current distribution is still assumed to be uniform. The simple method of approximating the sectors as being circular gives a useful estimate, but the more detailed representation using sub-conductors is assumed to be more accurate. Both analytical methods suggest lower reactances than in the manufacturer's data, with the zero sequence reactance approximately halved.

Table 3 Comparison of impedances from analysis with manufacturer's data for circuits with neutral as return path

Calculation technique	Positive sequence z_{11}, Ω/km	Zero sequence z_{00}, Ω/km
From manufacturer's data	0.32 + j0.0735	1.28 + j0.294
Analysis with sectors approximated as circles (Section 4.1)	0.32 + j0.057	1.28 + j0.116
Sectors modelled using sub-conductors (Section 4.2)	0.32 + j0.061	1.28 + j0.100
Adding corrections for AC resistance (Section 4.3)	0.323 + j0.061	1.283 + j0.100
Adding ground path in parallel with neutral (Section 4.4)	0.323 + j0.061	1.101 + j0.445
FE model for circuits with neutral and ground in parallel (Section 6.1)	0.322 + j0.060	1.096 + j0.450

Fig. 3 *Sub-conductor model of 3-core 95 mm² cable*

4.3 Analytical corrections for AC resistance

Standard IEC 60287 provides a means to determine the current ratings of cables and so includes methods to calculate the AC resistance of cables [29]. Although the equations are developed for circular conductors, compensation factors are included to allow for asymmetry in sector shapes. This method does not define the current distribution associated with the correction factors and so the reactance calculation here is still based on a uniform current distribution as above.

The standard defines the total AC resistance as

$$r_{i,\text{total}} = r_{i,\text{DC}}(1 + y_S + y_P)(1 + \lambda_1) \tag{17}$$

where y_S allows for the skin effect, y_P allows for the proximity effect and λ_1 allows for the resistive effect of losses due to eddy currents in the sheath.

The results in Table 3 for the 3-core 95 mm² cable show that the corrections make a minor difference to the impedance at 50 Hz.

The comparison has been repeated for the 3-core 300 mm² cable where the conductor dimensions are larger compared to the skin depth. Including the IEC 60287 corrections increase the positive sequence resistance by 6% (from 0.1 to 0.106 Ω/km). The corresponding parameters are then $y_S = 0.008$, $y_P = 0.014$ and $\lambda_1 = 0.04$ so the sheath losses give the greatest contribution.

4.4 Including the ground path

The impedances are now calculated using Carson's equations (10) and (11) to include the ground in parallel with the neutral. The resulting sequence impedances are shown in Table 3.

Adding the ground in parallel with the neutral does not affect the positive sequence impedance (with no unbalance current), but has reduced the zero sequence resistance by 14% and increased the zero sequence reactance by a factor of 4.

These results were also repeated for comparison using the 'full' Carson's equations [14], giving differences in the circuit impedances of <0.25% at 50 Hz, and <2% at 3 kHz. The differences are similar for all of the self-impedances and all of the mutual impedances, such that the resulting zero sequence impedances are almost identical with the full and modified Carson's equations.

5 FE model

The impedances obtained using the analytical techniques are now compared with results from FE analysis obtained using the FE method magnetics (FEMM) software [30]. This is freely available, such that it is possible for the results here to be replicated or extended in other work. The current distribution and magnetic field are solved for a planar cross-section of the conductor geometry, giving impedance results per unit length, and assuming an infinite longitudinal projection.

The geometry for the waveform cable was entered into FEMM using the sector outlines as described in Section 4.2, and drawing

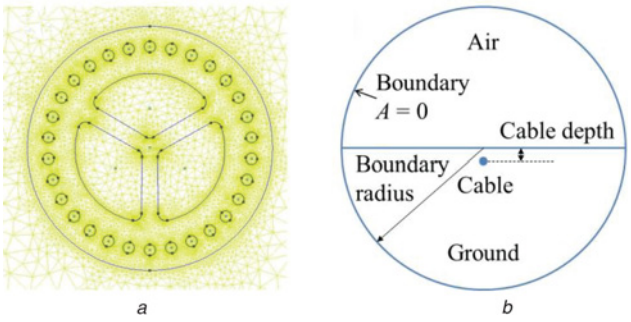

Fig. 4 *FEMM model showing of 3-core 95 mm² waveform cable*

a Conductors with mesh
b Ground conductor and boundary conditions

the neutral strands as circles. This defines a set of conducting regions placed within a non-conductive outer circle defined by the radius R_O of the cable, as shown in Fig. 4*a*. The voltage is constant across each conductor since the software only models longitudinal currents (a valid approximation for power frequencies).

Two further semi-circular regions were defined to represent the ground conductor surrounding the cable and the air above the ground surface, as shown in Fig. 4*b*. The ground resistivity is therefore constant over the planar cross-section. A boundary condition with magnetic vector potential $A = 0$ is applied at the edge of the solution space, effectively truncating the magnetic field at the boundary radius. A magnetic permeability of 1 was assumed throughout.

A separate simulation run was configured for each solution frequency and for each conductor. There are therefore 34 simulations for the 3-core 95 mm² cable (3 sectors, 30 neutral strands and the ground). In each run, a mean current of 1 A was applied to one 'active' conductor with the other conductors having a mean current of zero. This allows for eddy currents, but prevents currents from circulating between conductors (maintaining an open circuit at one end of the circuit, as shown in Fig. 1). Using default mesh parameters, the set of 34 simulation runs required less than 10 min.

For each run, the solver provides the self-impedance of the 'active' conductor and also the mutual inductance with each of the others. The mutual impedance has a complex value in which the imaginary term is negative and represents a resistive component in the mutual impedance, allowing for losses due to induced eddy currents.

It is again assumed that the dimensions of the cable lays are long relative to the conductor widths and spacings so that it is valid to model the conductors as being longitudinal when calculating the flux linkage. It has also been found that the mutual impedance between conductors and the ground is independent of their orientation.

The impact of the cable lay on the eddy currents needs further consideration since the sectors and neutral rotate relative to each other. At one position along the cable length, a strand will be adjacent to a particular sector conductor, but further along the cable it will be on the opposite side of the circle. Over a length of a few metres (and provided that the lay lengths are not exact multiples of each other), each strand has an approximately equal probability of being at any angle relative to the sector cores.

This transposing effect can be modelled by averaging the strand conductor impedances over the set of N_S strand positions around the cable. The mean self- or mutual conductor impedance for a strand is then

$$\bar{\bar{z}}_{ij} = \frac{1}{N_S}\sum_{k=0}^{N_S-1} \bar{z}_{i+k,j+k\ (\mathrm{mod}\ N_S)} \tag{18}$$

and the mutual impedance between sector i and strand j is

$$\bar{\bar{z}}_{ij} = \frac{1}{N_S}\sum_{k=0}^{N_S-1} \bar{z}_{i,j+k\ (\mathrm{mod}\ N_S)}. \tag{19}$$

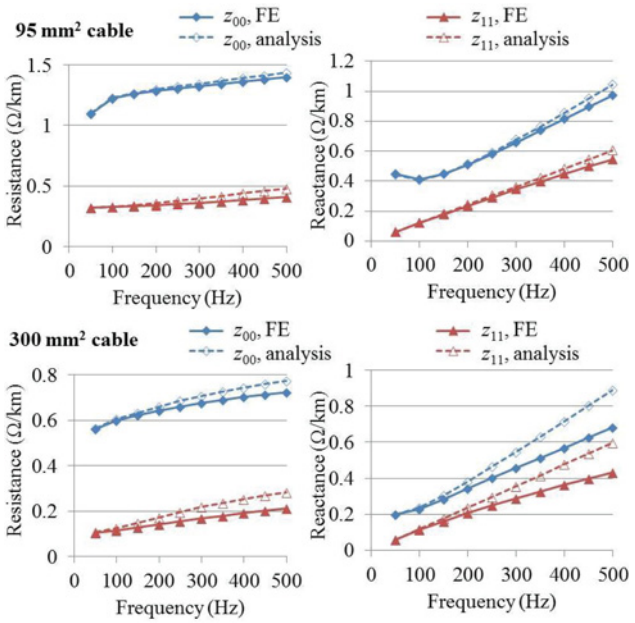

Fig. 5 *Positive (z_{11}) and zero (z_{00}) sequence impedances for 3-core 95 and 300 mm² cables*

These averaged conductor impedances are then used to calculate the impedances of circuits with a conductor and ground return according to (8) and (9). As in Section 2.2, the impact of the magnetic field truncation at the simulation boundary is then cancelled out in the resulting circuit impedances. This 4 × 4 matrix is then reduced to a 3 × 3 sequence impedance matrix, assuming a multi-grounded neutral as in Section 2.3.

6 Simulation results

6.1 Waveform cable impedances

The model was configured with the cable located 1 m below the ground surface, using ground resistivity of 100 Ωm, and with a 3 km simulation boundary radius. Using the DC resistance and cross-sectional area from Table 1, the conductor conductivity was defined as 33.9 MS/m for the aluminium sector and 53.1 MS/m for the copper neutral.

The FE simulations are compared with the analysis of Section 4.4, showing the impact of including a detailed representation of the current distribution in the cable. The ground is also modelled as a physical conductor rather than being included through analysis of the fields (as in Carson's equations). At 50 Hz, the sequence impedances from the FE simulations for the 95 mm² cable are within 1% of those obtained from the analysis, as shown in Table 3. At higher frequencies, the FE simulation results diverge from the analytical results, as shown in Fig. 5. At 450 Hz, the positive sequence impedance from the FE simulation has 16% lower resistance and 10% lower reactance. The corresponding zero sequence results are 3% lower for resistance and 6% lower for reactance.

Fig. 5 also shows the same comparison for the 300 mm² cable size where eddy currents would be expected to have greater impact. In this case, the results agree to within 2% at 50 Hz, but the positive sequence at 450 Hz has 33% lower resistance and reactance. The corresponding zero sequence results are 6% lower for resistance and 28% lower for reactance.

The results from the FE simulations support the conclusion that Carson's equations are valid for use with underground cables. Although differences arise between the FE results and the analysis results at higher frequencies, these are attributed to the limitations

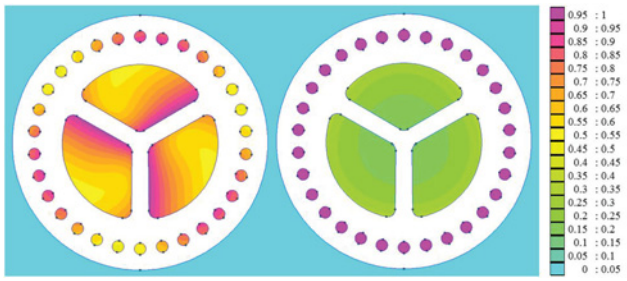

Fig. 6 *Relative current density from FEMM results, 350 Hz, 3-core 95 mm² cable*

a Positive sequence
b Zero sequence

of the AC resistance correction method which does not model the non-uniform current distribution within the cable conductors.

6.2 Three-phase current distributions

The FE model was re-configured with currents applied to each phase conductor so that the current distributions of the sequence modes could be observed. The neutral and ground conductors were configured in parallel to model a multi-grounded neutral. At 50 Hz, the current distribution was close to uniform and so the plots are shown for 350 Hz where the impact of eddy currents is more clearly visible.

Fig. 6*a* shows a FEMM plot of the current density for the positive sequence, where balanced three-phase currents of 1 A were applied to the sector conductors. The current density in the sectors is greatest on the edges orientated towards the sector leading in phase and the lowest on the opposite edge. This gives a higher resistance than for a uniform distribution.

The plot also shows eddy currents in the concentric neutral strands. These have a similar magnitude to those in the sectors and a phase angle that varies around the circle. However, the plot from a single cross-section represents the eddy currents that would occur if the strands remained at the same angle relative to the sectors for the full length of the cable. In practice, the currents in the strands are transposed as the cores rotate relative to the neutral due to the cable lay. This highlights a risk with FE models where this transposing effect is not taken into account.

A similar plot for the zero sequence at 350 Hz is shown in Fig. 6*b*. For this case, the model was configured with $1\angle 0°$ A in each sector and −3 A in the neutral and the ground. The current density in the sectors is slightly higher towards the outer edges, as expected due to the proximity effect. At 350 Hz, the current within the ground is negligible and almost all of the current returns through the neutral.

6.3 Ground conductor current distribution

For the simulations described above, the boundary radius was selected so that the ground conductor truncation did not significantly affect the results. As shown in Fig. 4*b*, the boundary limits the cross-sectional area of the ground, changing its DC resistance. This is a different concern with that noted in Section 2 where the truncation of the magnetic field is cancelled out when the currents inside the boundary sum to zero.

Fig. 7 shows sequence impedances for varying boundary radius. The positive sequence impedance is unaffected since this has no unbalance current, but a radius of at least 1 km is required for the zero sequence impedance at 50 Hz to converge. At higher frequencies, a lower radius can be used, as the increased proximity effect causes currents flowing in opposite directions (outwards via the cable and returning via the ground) to have a higher current density at closer separations.

A 1 km boundary radius may seem large, but is consistent with the dimensions implied by Carson's equations, in which the self-impedance term $\mu_0\omega/8$ represents the additional resistance of a circuit with a ground return. At 50 Hz, with ground resistivity of 100 Ωm, an equivalent resistance would be provided by a semi-circular conductor with a radius of 1136 m. This suggests that the ground current for short LV cables would be subject to significant end effects. Where unbalance current enters the ground at earth electrodes, the current density is much greater, and the ground path resistance much higher than in the infinite longitudinal projection, giving the high grounding resistances noted in [2]. In the absence of a three-dimensional network model, this suggests that it would better to approximate the neutral as being isolated from the ground, rather than to apply Carson's equations and then a zero impedance connection between the neutral and the ground.

6.4 Impact of ground resistivity and cable depth

To determine the sensitivity of the FE model to ground resistivity, the simulations have been repeated with resistivity increased or decreased by a factor of 10, as shown in Table 4. A higher boundary radius of 30 km was used here to allow for the higher ground resistivity. The zero sequence impedance varies from 3 to 4% for each order of magnitude change, and so is relatively insensitive to variations in the ground resistivity.

The simulations were repeated with the cable position varied between 2 m below ground and 2 m above, with the results remaining within 0.1% of the values shown in Table 4. Since the current distribution within the ground reduces gradually over hundreds of metres, a relatively small difference in the cable position has minimal impact.

7 Conclusions

Accurate cable impedance data is needed to evaluate the impacts of connecting new low carbon technologies to LV networks. Published studies have adopted a range of impedance models with differing approaches used to represent the geometry of the conductors and the current distribution within them. This paper compares the manufacturer's data for 3-core waveform cable with impedances calculated using analytical techniques, showing the differences that arise as the complexity of the model is increased.

In the simplest analytical model, the sector shapes were approximated as being circular with uniform current distribution and no connection to the ground. Representing the sector shapes more accurately by using a grid of sub-conductors gave a difference in the reactance at 50 Hz of 14%, suggesting that the more detailed geometry representation is needed for more accurate results. Including the AC resistance corrections from IEC 60287 had minimal impact at 50 Hz for the 95 mm² cable, although a 6% difference was noted for the 300 mm² cable size. The reactance results from all of the analytical techniques were lower than those indicated by the manufacturer. The addition of the ground path in parallel with the neutral affected the zero sequence impedance

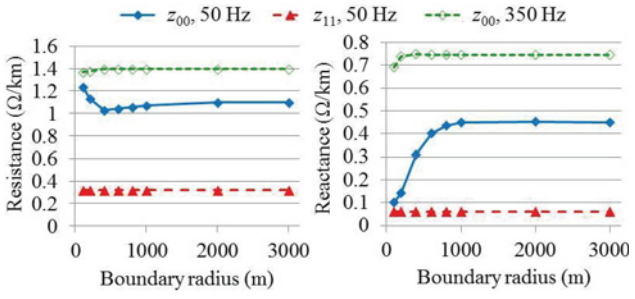

Fig. 7 *Positive (z_{11}) and zero (z_{00}) sequence impedances versus boundary radius, 3-core 95 mm² cable, ground resistivity of 100 Ωm, cable located 1 m below the surface*

Table 4 Zero sequence impedance at 50 Hz for 3-core 95 mm^2 cable

Ground resistivity, Ωm	Zero sequence impedance, Ω/km
10	1.062 + 0.469j
100	1.096 + 0.450j
1000	1.122 + 0.430j

with a 14% reduction in the resistance and a 4x increase in the reactance.

The use of a freely-available FE solver (FEMM) is then described as an accurate means of allowing for the sector-shape geometry and for the non-uniform current distribution due to induced eddy currents. The results at 50 Hz matched those from the analytical methods to within 1% so there was little to be gained from the more complex FE approach. However, at harmonic frequencies, the FE results diverge from the results with the IEC 60287 corrections, with differences at 450 Hz of 16% for the 95 mm^2 cable and 33% for the 300 mm^2 cable. The use of the FE model would therefore be recommended where accurate impedance data is required at harmonic frequencies. The results are available for download from [21].

At 50 Hz, the FE results are consistent with those obtained from the modified form of Carson's equations, providing confidence in their use for underground cables. The FE results were relatively insensitive to variations in ground resistivity and were unaffected by likely variations in the depth of the cable within the ground.

However, both the FE model and Carson's equations assume an infinite longitudinal projection of the current distribution. Examination of the implied current distribution suggests that the ground path will be subject to much higher resistance where unbalance current enters the ground at earthing electrodes. For short LV cables, the grounding resistance would be significantly higher than that of the neutral conductor. This suggests that modelling the neutral as isolated from the ground would be a better approximation than using Carson's equations and then assuming a perfect short circuit between the neutral and the ground when applying the Kron reduction.

8 Acknowledgments

This work was supported by the Engineering and Physical Sciences Research Council (EPSRC), UK (EP/I031707/1 and voucher 11220756) and by E.ON Technologies (Ratcliffe) Limited, UK.

9 References

1 Miu, K., Kleinberg, M.: 'Impact studies of unbalanced multi-phase distribution system component models'. IEEE PES General Meeting, 2010, pp. 1–4
2 Sunderland, K.M., Conlon, M.F.: '4-Wire load flow analysis of a representative urban network incorporating SSEG'. 47th Int. Universities Power Engineering Conf., September 2012, pp. 1–6
3 Collins, E.R., Jiang, J.: 'Analysis of elevated neutral-to-earth voltage in distribution systems with harmonic distortion', *IEEE Trans. Power Deliv.*, 2009, **24**, (3), pp. 1696–1702
4 Prysmian: 'Low voltage waveform cable', http://www.uk.prysmiangroup.com/en/business_markets/markets/pd/downloads/datasheets/Waveform.pdf, accessed April 2015
5 Weckx, S., Driesen, J.: 'Load balancing with EV chargers and PV inverters in unbalanced distribution grids', *IEEE Trans. Sustain. Energy*, 2015, **6**, (2), pp. 635–643
6 Mott McDonald: 'System integration for additional micro-generation', http://www.webarchive.nationalarchives.gov.uk/+/http://www.dti.gov.uk/renewables/publications/pdfs/dgcg00028rep.pdf, accessed April 2015
7 Thomson, M., Infield, D.G.: 'Network power-flow analysis for a high penetration of distributed generation', *IEEE Trans. Power Syst.*, 2007, **22**, (3), pp. 1157–1162
8 Frame, D.F., Ault, G.W., Huang, S.: 'The uncertainties of probabilistic LV network analysis'. IEEE Power and Energy Society General Meeting, 2012, pp. 1–8
9 Kersting, W.H., Phillips, W.H.: 'Distribution feeder line models', *IEEE Trans. Ind. Appl.*, 1995, **31**, (4), pp. 715–720
10 Navarro-Espinosa, A., Mancarella, P.: 'Probabilistic modeling and assessment of the impact of electric heat pumps on low voltage distribution networks', *Appl. Energy*, 2014, **127**, pp. 249–266
11 Akmal, M., Fox, B., Morrow, J.D., *et al.*: 'Impact of heat pump load on distribution networks', *IET Gener. Transm. Distrib.*, 2014, **8**, (12), pp. 2065–2073
12 Carson, J.R.: 'Wave propagation in overhead wires with ground return', *Bell Syst. Tech. J.*, 1926, **5**, (4), pp. 539–554
13 Kersting, W.H.: 'Distribution system modeling and analysis' (CRC Press, 2012)
14 Kersting, W.H., Green, R.K.: 'The application of Carson's equation to the steady-state analysis of distribution feeders'. IEEE/PES Power Systems Conf. and Exposition, 2011, pp. 1–6
15 Wedepohl, L.M., Wilcox, D.J.: 'Transient analysis of underground power-transmission systems. System-model and wave-propagation characteristics', *Proc. Inst. Electr. Eng.*, 1973, **120**, (2), p. 253
16 Høgdahl Jensen, M., Bak-Jensen, B.: 'Series impedance of the four-wire distribution cable with sector-shaped conductors'. IEEE Power Tech Proc., Porto, Portugal, September 2001, p. 6
17 Du, Y., Burnett, J.: 'Experimental investigation into harmonic impedance of low-voltage cables', *IEE Proc., Gener. Transm. Distrib.*, 2000, **147**, (6), p. 322
18 Marshall, J.S., Hines, P.D., Zhang, J.D., *et al.*: 'Modeling the impact of electric vehicle charging on heat transfer around underground cables', *Electr. Power Syst. Res.*, 2013, **97**, pp. 76–83
19 Yin, Y.: 'Calculation of frequency dependent parameters of underground cables with finite element method'. PhD thesis, University of British Columbia, 1990
20 Rivas, R.A., Marti, J.R.: 'Calculation of frequency-dependent parameters of power cables: matrix partitioning techniques', *IEEE Trans. Power Deliv.*, 2002, **17**, (4), pp. 1085–1092
21 Urquhart, A.J., Thomson, M.: 'Cable impedance data', https://www.dspace.lboro.ac.uk/2134/15544
22 Høgdahl Jensen, M., Bak-Jensen, B.: 'Shunt admittance of the four-wire distribution cable with sector-shaped conductors'. Proc. of AUPEC 2001, Perth, Australia, September 2001, p. 6
23 Glover, J.D., Sarma, M.S., Overbye, T.J.: 'Power system analysis and design' (Cengage Learning, 2008, 4th edn.)
24 Rosa, E.B.: 'On the geometrical mean distances of rectangular areas and the calculation of self-inductance', *Bull. Bur. Stand.*, 1907, **3**, (1), p. 41
25 BS 3988:1970: 'Wrought aluminium for electrical purposes – Solid conductors for insulated cables', 1970
26 BS 7870-3.40:2001: 'LV and MV polymeric insulated cables for use by distribution and generation utilities', 2001
27 BS 7870-3.40:2011: 'LV and MV polymeric insulated cables for use by distribution and generation utilities', 2011
28 Beharrysingh, S.: 'Phase unbalance on low voltage networks and its mitigation using static balancers'. PhD thesis, Loughborough University, 2014
29 BS IEC 60287-1-1:2006: 'Electric cables – calculation of the current rating', 2006
30 Meeker, D.: 'Finite element method magnetics version 4.2 user manual'. http://www.femm.info/Archives/doc/manual42.pdf, accessed April 2015